LETTER

Telomerase reactivation reverses tissue degeneration in aged telomerase–deficient mice

Mariela Jaskelioff[1], Florian L. Muller[1], Ji–Hye Paik[1], Emily Thomas[1], Shan Jiang[1], Andrew C. Adams[2], Ergun Sahin[1], Maria Kost-Alimova[1], Alexei Protopopov[1], Juan Cadiñanos[1], James W. Horner[1], Eleftheria Maratos–Flier[2] & Ronald A. DePinho[1]

An ageing world population has fuelled interest in regenerative remedies that may stem declining organ function and maintain fitness. Unanswered is whether elimination of intrinsic instigators driving age-associated degeneration can reverse, as opposed to simply arrest, various afflictions of the aged. Such instigators include progressively damaged genomes. Telomerase-deficient mice have served as a model system to study the adverse cellular and organismal consequences of wide-spread endogenous DNA damage signalling activation *in vivo*[1]. Telomere loss and uncapping provokes progressive tissue atrophy, stem cell depletion, organ system failure and impaired tissue injury responses[1]. Here, we sought to determine whether entrenched multi-system degeneration in adult mice with severe telomere dysfunction can be halted or possibly reversed by reactivation of endogenous telomerase activity. To this end, we engineered a knock-in allele encoding a 4-hydroxytamoxifen (4-OHT)-inducible telomerase reverse transcriptase-oestrogen receptor (TERT-ER) under transcriptional control of the endogenous TERT promoter. Homozygous TERT-ER mice have short dysfunctional telomeres and sustain increased DNA damage signalling and classical degenerative phenotypes upon successive generational matings and advancing age. Telomerase reactivation in such late generation TERT-ER mice extends telomeres, reduces DNA damage signalling and associated cellular checkpoint responses, allows resumption of proliferation in quiescent cultures, and eliminates degenerative phenotypes across multiple organs including testes, spleens and intestines. Notably, somatic telomerase reactivation reversed neurodegeneration with restoration of proliferating Sox2^{+} neural progenitors, Dcx^{+} newborn neurons, and Olig2^{+} oligodendrocyte populations. Consistent with the integral role of subventricular zone neural progenitors in generation and maintenance of olfactory bulb interneurons[2], this wave of telomerase-dependent neurogenesis resulted in alleviation of hyposmia and recovery of innate olfactory avoidance responses. Accumulating evidence implicating telomere damage as a driver of age-associated organ decline and disease risk[1,3] and the marked reversal of systemic degenerative phenotypes in adult mice observed here support the development of regenerative strategies designed to restore telomere integrity.

Accelerating structural and functional decline across diverse organ systems is observed in the aged[1,3,4]. The loss of genome integrity and associated DNA damage signalling and cellular checkpoint responses are well-established intrinsic instigators that drive tissue degeneration during ageing[5]. Of particular relevance to this study, age-progressive loss of telomere function in mice has been shown to provoke widespread p53 activation resulting in activation of cellular checkpoints of apoptosis, impaired proliferation and senescence, compromised tissue stem cell and progenitor function, marked tissue atrophy and physiological impairment in many organ systems[1,6].

Mounting evidence in humans has also provided strong association of limiting telomeres with increased risk of age-associated disease[7] and with onset of tissue atrophy and organ system failure in degenerative diseases such as ataxia-telangiectasia, Werner syndrome, dyskeratosis congenita and liver cirrhosis, among others[1,3]. In cell-based models of ataxia-telangiectasia and Werner syndrome, enforced TERT can restore normal cellular proliferative potential[8]. These findings build on seminal cell culture studies showing that enforced TERT expression can endow primary human cells with unlimited replicative potential[9]. Importantly, TERT overexpression in epithelial tissues of cancer-resistant mice leads to extended median lifespan[10]. In addition, intercrossing wild-type and late generation *mTerc*^{−/−} mice with severe degenerative phenotypes results in healthy offspring[11], indicating that viable late generation *mTerc*^{−/−} germ cells can be restored to normal telomere function on introduction of a wild-type *mTerc* allele at the time of fertilization. However, to our knowledge, there are no genetic or pharmacological studies showing somatic reversal of age-related degenerative phenotypes driven by endogenous genotoxic stresses in adult mammals. Here, in telomerase-deficient mice experiencing severe tissue degeneration, we investigated whether endogenous telomerase-mediated restoration of telomere function throughout the organism would quell DNA damage signalling and either arrest, or possibly reverse, cellular checkpoint responses and associated tissue atrophy and dysfunction. Notably, the mice enlisted into this study are adults exhibiting significant progeroid phenotypes.

Construction and functional validation of the germline TERT-ER knock-in allele are detailed in Supplementary Fig. 1. In the absence of 4-OHT, ER fusion proteins remain in an inactive misfolded state[12] and thus we first sought to verify whether mice homozygous for TERT-ER recapitulated the classical premature ageing phenotypes of mice null for *mTerc* or *mTert*. To that end, mice heterozygous for TERT-ER (hereafter G0[TERT-ER]) were intercrossed to produce first generation mice homozygous for TERT-ER (G1[TERT-ER]) which were then intercrossed to produce successive G2, G3 and G4[TERT-ER] cohorts. G1–G4[TERT-ER] cells have no detectable telomerase activity (Fig. 1a). Accordingly, G4[TERT-ER] primary splenocytes had hallmark features of short dysfunctional telomeres, including decreased telomere-specific fluorescence *in situ* hybridization (FISH) signal and Robertsonian fusions (Fig. 1b, e, f). Moreover, G4[TERT-ER] fibroblasts failed to divide after five to six passages and adopted a flat, senescence-like morphology (Fig. 1c, d). Adult G4[TERT-ER] mice showed widespread tissue atrophy, particularly in highly proliferative organs including extreme testicular atrophy and reduced testes size due to apoptotic elimination of germ cells, resulting in decreased fecundity (Fig. 2a, d and Supplementary Fig. 2a), marked splenic atrophy with accompanying increased 53BP1 (also known as Trp53bp1) foci consistent with DNA damage (Fig. 2b, e, h) and intestinal crypt depletion and villus atrophy in conjunction with numerous apoptotic crypt cells and increased 53BP1 foci (Fig. 2c, f, i and Supplementary Fig. 2b). Finally, median survival of G4[TERT-ER] mice is significantly decreased relative to that of telomere intact mice (43.5 versus 86.8 weeks, ***$P < 0.0001$, Supplementary Fig. 2f). Thus, G4[TERT-ER] mice phenocopy late generation *mTert*^{−/−} and *mTerc*^{−/−} animals[13,14], indicating that TERT-ER is inactive in the absence of 4-OHT.

[1]Belfer Institute for Applied Cancer Science and Departments of Medical Oncology, Medicine and Genetics, Dana-Farber Cancer Institute, Harvard Medical School, Boston, Massachusetts 02115, USA. [2]Division of Endocrinology, Diabetes & Metabolism, Beth Israel Deaconess Medical Center, Harvard Medical School, Boston, Massachusetts 02215, USA.
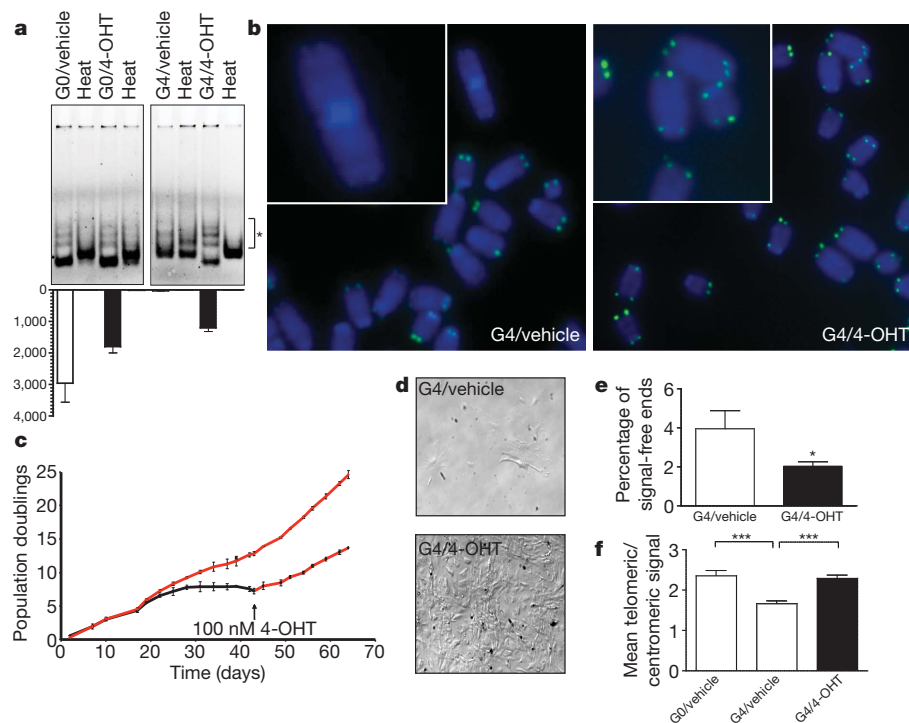
Figure 1 | 4-OHT-dependent induction of telomerase activity in TERT-ER cells. **a**, Telomerase activity in eNSCs (*, telomerase products) (top); real-time quantification of reactions above (bottom). **b**, Representative G4[TERT-ER] splenocyte metaphases. **c**, Proliferation of adult G4[TERT-ER] fibroblasts ($n = 3$) in media with vehicle (black) or 4-OHT (red). **d**, Representative image of G4[TERT-ER] fibroblasts (passage 6) in media with 4-OHT (bottom) or vehicle (top). **e**, Signal-free ends in primary splenocyte metaphases, 15 metaphases per sample, $n = 2$ (*$P < 0.05$). **f**, Mean telomere-FISH signal in primary splenocyte interphases, normalized to centromeric signal, $n = 3$ (***$P < 0.0001$). Open bars correspond to vehicle-treated and filled bars to 4-OHT-treated, error bars represent s.d.

Next, we assessed the impact of telomerase reactivation on telomere dysfunction-induced proliferative arrest. On passage of adult G4[TERT-ER] fibroblast cultures, cells adopted flat senescent-like morphology at approximately five population doublings (Fig. 1d, upper panel). These quiescent cultures showed prominent G0/G1 accumulation in the cell cycle by fluorescence-activated cell sorting (FACS) analysis and rare cell division events by time-lapse video microscopy (not shown). However, upon replating these cells in media containing 100 nM 4-OHT, telomerase reactivation led to elongated telomeres, prompt resumption of proliferation over greater than eight additional passages tested, and reduction in the G0/G1 phase fraction (Fig. 1c; data not shown). Coincidently, high levels of cyclin-dependent kinase inhibitor, p21[CIP1] (also known as Cdkn1a), declined upon 4-OHT treatment of the G4[TERT-ER] cultures, allowing cell cycle re-entry (Supplementary Fig. 2e). This pattern of p21[CIP1] regulation aligns with previous work documenting its role as a key mediator of cell cycle arrest induced by telomere dysfunction in mouse tissues[15]. Parallel G0 or G4[TERT-ER] fibroblasts maintained in 4-OHT at initial isolation did not undergo passage-induced senescence and instead showed sustained proliferation (>20 passages; Fig. 1c, d).

These cell-based studies prompted systemic analyses of the impact of 4-OHT-mediated telomerase reactivation in the setting of entrenched tissue degeneration. At the end of 4 weeks of continuous 4-OHT exposure, documentation of telomerase-mediated telomere restoration and function in G4[TERT-ER] tissues included increased telomere-FISH signal in primary splenocytes (Fig. 1b, e, f), decreased p53 activation and expression of p21[CIP1] in liver (Supplementary Fig. 2d, e), and marked decrease in 53BP1 foci in splenocytes (Fig. 2b, e) and intestinal crypt cells (Fig. 2c, f). These molecular changes paralleled striking tissue rejuvenation including reduced apoptosis of testes germ cells (data not shown) and intestinal crypt cells (Supplementary Fig. 2b, i), reduced tissue atrophy with restoration in normal testes and spleen size (Fig. 2d, h and Supplementary Fig. 2a) and, most strikingly, increased fecundity (Fig. 2g). Moreover, median survival increased in G4[TERT-ER] mice treated with a 4-week course of 4-OHT (**$P < 0.005$, Supplementary Fig. 2f). Sustained 4-OHT treatment had no effect on G0[TERT-ER] age- and gender-matched controls which were included in all experiments. Together, these data indicate that, despite an entrenched degenerative state, endogenous telomerase reactivation results in marked extinction of DNA damage signalling, alleviation of cellular checkpoint responses and reversal of tissue atrophy in highly proliferative organ systems of the late generation TERT-ER mice.

Although the marked impact of telomerase reactivation on highly proliferative organs is encouraging, we sought to assess more intensively the potential benefits on brain health, which is a prime determinant of age-progressive declining health in humans. Along these lines, it is worth noting that the ageing mammalian brain shows accumulating DNA damage[16] and a progressive restriction of neurogenesis and impaired re-myelination due to a decline in neural stem and progenitor cell proliferation and differentiation[17]. As neural stem/ progenitor cells (hereafter NSCs) support neurogenesis, particularly in the subventricular zone (SVZ), we first examined the properties of NSCs derived from adult G0 and G4[TERT-ER] mice. As reported previously for late generation $mTerc^{-/-}$ mice[6,14,18], vehicle-treated G4[TERT-ER] NSC cultures showed decreased self-renewal activity relative to G0[TERT-ER] controls and this defect was partially corrected with 4-OHT treatment (Fig. 3a, d). G4[TERT-ER] neurospheres were not only rarer but also smaller in diameter than G0[TERT-ER] controls, and their average diameter was restored to normal by 4-OHT treatment (Fig. 3a and Supplementary Fig. 2c). These self-renewal profiles tracked with activated p53-mediated DNA damage signalling in vehicle-treated G4[TERT-ER] NSC cultures, which was extinguished with 4-OHT treatment and absent in the G0[TERT-ER] controls (Fig. 3b, e). Examination of NSC differentiation capacity revealed significant (twofold) reduction in G4[TERT-ER] NSC capacity to generate neurons relative to 4-OHT-treated G4[TERT-ER] cultures and 4-OHT- or vehicle-treated G0[TERT-ER] controls (Fig. 3c, f). Consistent with previous work[14,18], there was no impact on astrocyte differentiation (data not shown).

On the basis of these cell culture observations, we examined the SVZ, a region where NSCs reside and have an active role in adult brain physiology. In adult mice, NSCs give rise to transit-amplifying progenitor cells that divide rapidly and contribute to generation of neuroblasts, astrocytes and myelinating oligodendrocytes. Consistent with previous reports of an SVZ proliferation defect in $mTerc^{-/-}$ mice[6,14,18] and wild-type aged mice[19], vehicle-treated G4[TERT-ER] mice show a profound decrease in proliferating (Ki67^{+}) cells in the SVZ relative to G0[TERT-ER] controls. Notably, 4-OHT-treated G4[TERT-ER] mice show a striking, albeit partial, restoration of proliferation following only
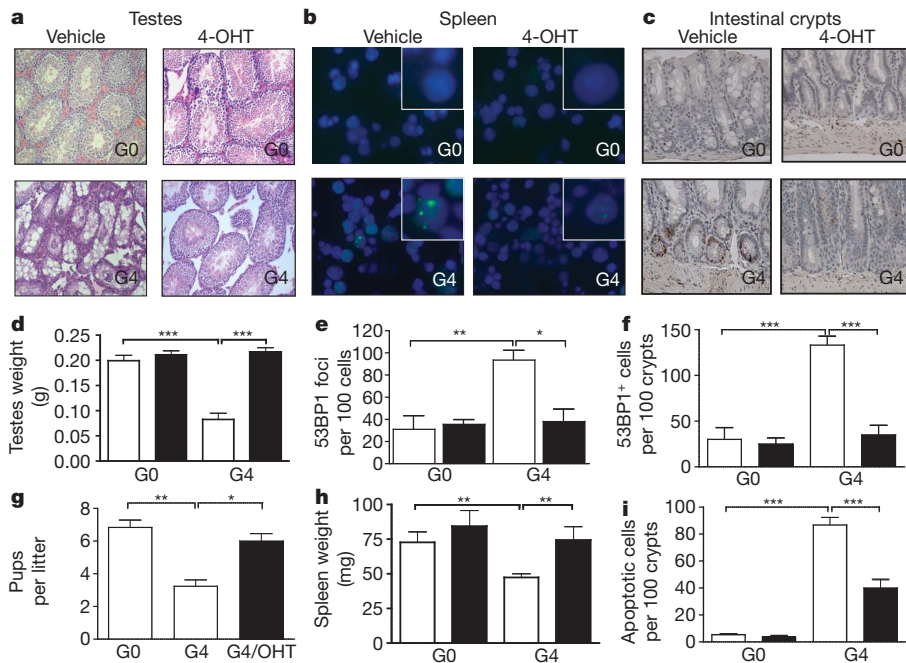
Figure 2 | Telomerase activation in adult TERT-ER mice. a–c, Representative images of tissues from experimental and control mice. **a**, Haematoxylin and eosin-stained sections of testes. **b**, Primary splenocytes stained for 53BP1. **c**, Small intestine sections stained for 53BP1. **d**, Testes weight of adult males (30–50-week-old, $n \geq 10$). **e**, 53BP1 nuclear foci per 100 nuclei ($n = 3$). **f**, 53BP1 nuclear foci per 100 crypts ($n = 4$). **g**, Litter sizes ($n = 3$); **h**, Spleen weights ($n \geq 6$). **i**, Apoptotic cells per 100 intestinal crypts ($n \geq 20$). $***P = 0.0001$, $**P < 0.005$, $*P < 0.05$. Open bars correspond to vehicle-treated and filled bars to 4-OHT-treated groups, error bars represent s.d.

4 weeks of treatment (Fig. 4, first row). This resumed SVZ proliferation mirrors well restoration of $Sox2^+$ cells, a marker of NSCs (Fig. 4, second row), and doublecortin (Dcx)-positive cells, an early neuronal lineage marker, together demonstrating preservation of neural stem/progenitor reserves and their neurogenic capacity *in vivo* (Fig. 4, third row). Finally, quantitative FISH analysis shows telomere elongation in the SVZ after 4 weeks of 4-OHT treatment (Supplementary Fig. 3). Thus, the markedly constrained neural progenitor proliferation and neurogenesis profile associated with telomere dysfunction can be ameliorated by reactivation of endogenous telomerase activity.

To test the hypothesis that telomerase reactivation leads to tissue rejuvenation, we conducted detailed morphological and functional fitness analyses of different brain structures upon telomerase reactivation. First, we examined the white matter of the corpus callosum and observed that aged $G4^{TERT-ER}$ mice have far fewer $Olig2^+$ mature oligodendrocytes (Fig. 4, fourth row). This cellular deficiency is associated with reduced brain weight (Fig. 5a, b) and significantly thinner myelin sheathing of neurons with g ratios (numerical ratio between the diameter of the axon proper and the outer diameter of the myelinated fibre) of 0.7756 ± 0.0054 for $G4^{TERT-ER}$ mice versus 0.7032 ± 0.0049 for $G0^{TERT-ER}$ (mean ± s.e.m., $***P < 0.0001$) (Fig. 5c, d). Remarkably, endogenous telomerase reactivation reinstates normal numbers of mature oligodendrocytes (Fig. 4) and reverses the hypomyelination

phenotype at the level of mean myelin sheath diameters (with g ratios of 0.7058 ± 0.0006 and 0.7164 ± 0.0063 for 4-OHT-treated G4 and $G0^{TERT-ER}$ mice, respectively) (Fig. 5c, d). Furthermore, a 4-OHT treatment course of only 4 weeks is sufficient to cause significant partial reversion of the brain size defect, with $G4^{TERT-ER}$ brain weights increasing from $77.3 \pm 3.3\%$ of $G0^{TERT-ER}$ brain weights in the vehicle group to $89.7 \pm 4.0\%$ in the 4-OHT group (Fig. 5a, b). Importantly, telomere elongation can be detected in the corpus callosum after 4 weeks of telomerase reactivation (Supplementary Fig. 3c). Thus, endogenous telomerase reactivation exerts a swift impact on oligodendrocyte proliferation and differentiation, and promotes repopulation of white matter structures with mature oligodendrocytes and active myelin deposition.

Lastly, we investigated the physiological effect of telomere dysfunction and telomerase reactivation on olfactory function. Age-associated hyposmia, as evidenced by an increased olfactory threshold and a reduced ability in odour identification and discrimination, is a well established phenomenon in aged humans[20]. In rodents, ageing is associated with diminished olfactory neurogenesis and deficits in fine olfactory discrimination[19,21]. Olfactory interneurons in the olfactory bulb that receive and process information from the olfactory sensory neurons in the olfactory epithelium derive from SVZ stem cells[2]. Rodents demonstrate avoidance responses towards predators' odorants as well as spoiled smells like aliphatic acids, aliphatic aldehydes and alkyl amines, which are
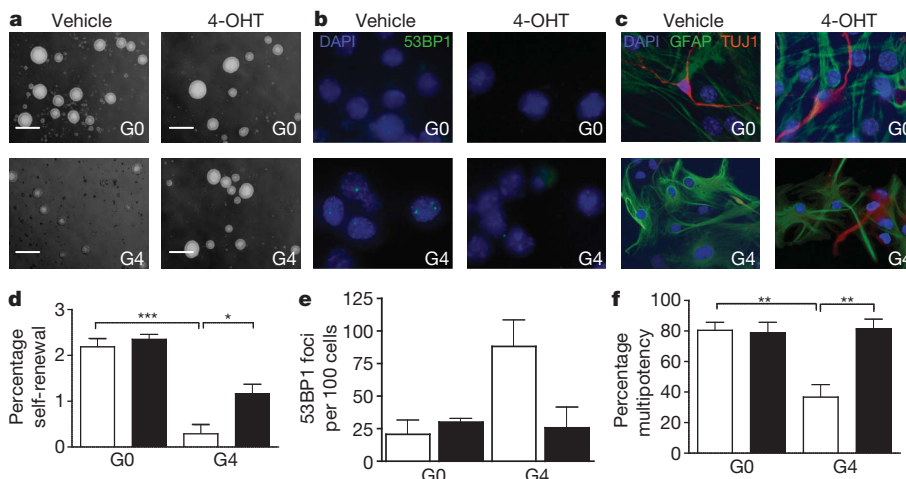

Figure 3 | Neural stem cell function following telomerase reactivation *in vitro*. a–c, Representative images of experimental and control mice-derived NSCs. **a**, Secondary neurospheres. **b**, Differentiated NSCs stained with 53BP1 or **c**, GFAP and TUJ1 antibodies. **d**, Self-renewal capacity of secondary neurospheres ($n = 4$) $***P < 0.0001$, $*P < 0.001$. **e**, 53BP1 nuclear foci per 100 cells (>400 nuclei per culture, $n = 3$). **f**, Multipotency ($GFAP^+/TUJ1^+$) of NSCs ($n = 4$; 308 wells per culture condition) $**P = 0.0066$. Scale bar, 100 μm. Open bars correspond to vehicle-treated and filled bars to 4-OHT-treated groups, error bars represent s.d.

Figure 4 | NSC proliferation and differentiation following telomerase reactivation *in vivo.* NSC proliferation and neurogenesis were measured by Ki67, Sox-2 and Dcx expression in SVZ from experimental and control mice. Mature oligodendrocytes in the corpus callosum were stained with anti-Olig2 antibody. Equivalent coronal sections ($n > 10$) were scored in a blinded fashion by laser scanning and plotted on the right panels. $\times 20$ (SVZ) or $\times 40$ (corpus callosum) objectives were used. *** $P < 0.0001$, ** $P = 0.0022$. Open bars correspond to vehicle-treated and filled bars to 4-OHT-treated groups, error bars represent s.d.
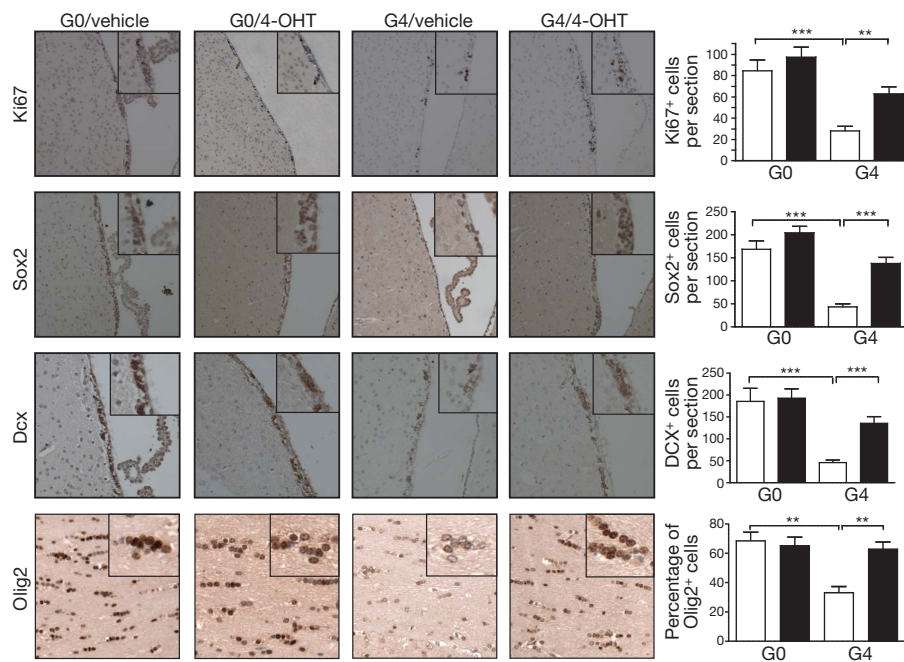
processed in the olfactory bulb[22]. Given the marked decrease in SVZ neurogenesis of G4$^{TERT-ER}$ mice and the fact that the olfactory bulb retains high telomerase activity in adult wild-type mouse brains[23], we sought to determine whether telomere dysfunction results in a functional deficit of these mice to detect and process odorants for elicitation of instinctive avoidance/defensive behaviours.

Pathology within the olfactory epithelium which may be considered a basis of age-related olfactory dysfunction, was ruled out by confirmation of grossly normal histology of the olfactory epithelium in both cohorts (Supplementary Fig. 4). Next, we ruled out alterations in exploration behaviour and overall locomotion by monitoring total distance travelled by the animals in the absence of odorants, which was similar for all experimental groups (Supplementary Table 1; Fig. 5e). We then performed innate avoidance tests using serially diluted 2-methylbutyric acid (2-MB), an odorant that rouses innate aversive responses in mice. Whereas G0$^{TERT-ER}$ mice demonstrated avoidance

responses at all 2-MB concentrations tested (1.87×10^{-4} M to 1.87×10^{-6} M), G4 mice showed attraction/neutral behaviours at concentrations lower than 1.87×10^{-4} M (Fig. 5e, f). Strikingly, following only 4 weeks of 4-OHT treatment, the performance of G4$^{TERT-ER}$ mice was markedly improved, with avoidance behaviours being apparent at all 2-MB concentrations (Fig. 5e, g). Accordingly, the frequency of entry into the odour zone was higher for vehicle-treated G4$^{TERT-ER}$ mice than for the other three experimental groups (Supplementary Table 2). These findings are consistent with significant alleviation of the olfactory defect stemming from the documented wave of telomerase-mediated SVZ neurogenesis and oligodendrocyte maturation which would promote repopulation of olfactory bulbs with functional interneurons and improve olfactory neuron function via remyelination.

Here, we report the generation of a novel mouse model to explore the impact of physiological telomerase reactivation across diverse adult cell types and organ systems. In G4$^{TERT-ER}$ mice with advanced degenerative
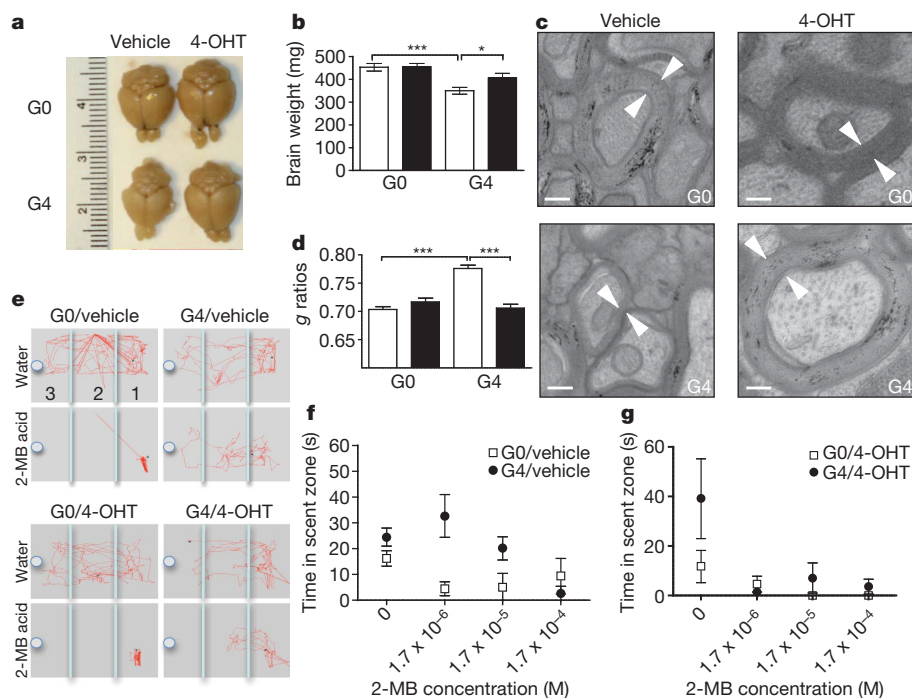

Figure 5 | Brain size, myelination, and olfactory function following telomerase reactivation. **a,** Representative brains from age-matched experimental and control animals. **b,** Brain weights, $n \geq 10$, ***$P = 0.0004$, *$P = 0.02$. **c,** Representative electron micrographs of myelinated axonal tracts in corpus callosum, arrow heads indicate myelin sheath width ($\times 12,000$). Scale bars, 200 nm. **d,** g ratios (inner/outer radii) ($n = 2$, >150 axons per mouse) ***$P < 0.0001$. **e,** Representative tracings of experimental and control mice during 3-min exposure to water or 2-MB. **f, g,** Time spent in scent zone 3 with water or 2-MB for vehicle- or 4-OHT-treated G0$^{TERT-ER}$ (squares) and G4$^{TERT-ER}$ (circles) mice; $n = 4$. Error bars represent s.d., except in (**d**) (s.e.m.).

phenotypes, short-term telomerase reactivation restored telomere reserves, quelled DNA damage signalling, and alleviated cellular checkpoint responses in several high-turnover organ systems with significant functional impact including increased fecundity. From this, we speculate that some tissue stem/progenitor cells are retained in a quiescent and intact state yet can be enlisted to resume normal repopulating function upon elimination of genotoxic stress at telomeres. Despite chromosomal instability, the brief course of telomerase reactivation was not sufficient to promote carcinogenesis (data not shown), a finding consistent with a role for telomerase in promoting progression of established neoplasms[24]. However, it remains possible that more prolonged telomerase reactivation schedules or applications in later life may provoke carcinogenesis.

As noted, age-associated compromise in mammalian brain function is associated with extensive accumulation of DNA damage and progressive reduction in neurogenesis and myelination. Indeed, many aspects of this central nervous system decline are accelerated and worsened in the setting of telomere dysfunction (refs 25, 26, this study). Our data establish that telomerase reactivation in adult mice with telomere dysfunction can restore SVZ neurogenesis and, consistent with its role in sustaining new olfactory bulb neurons, can ameliorate odour detection with improved performance in innate odour avoidance tests. These results are consistent with previous studies showing that prolonged inhibition of neurogenesis in the SVZ has a negative effect on odour detection thresholds[27]. In conclusion, this unprecedented reversal of age-related decline in the central nervous system and other organs vital to adult mammalian health justify exploration of telomere rejuvenation strategies for age-associated diseases, particularly those driven by accumulating genotoxic stress.

METHODS SUMMARY

TERT-ER mice were generated with traditional knock-in methods and following standard breeding protocol of successive generations of telomerase-deficient mice[13]. All studies were performed on adult males. 4-OHT time-release pellets (2.5 mg; Innovative Research of America) were inserted subcutaneously to reach steady state blood levels of 1 ng ml^{-1} 4-OHT. For neurosphere assays, SVZs were dissected, dispersed into a single-cell suspension and plated in neurobasal media supplemented with EGF, bFGF and 100 nM 4-OHT or vehicle. For multipotentiality assays, neurospheres were transferred to differentiation media (1% FBS). For histological studies, mice were perfused with 10% formalin; equivalent coronal sections were stained with indicated antibodies following standard immunohistochemistry protocol. Laser scanning cytometric quantification was performed with an iCys Research Imaging Cytometer (Compucyte). For innate olfactory avoidance tests, mice were fasted for 20 h and habituated for 20 min to the test cage where their responses were recorded on a video camera mounted above the test chamber. A filter paper scented with water or progressively higher concentrations of 2-methylbutyric acid was placed in the cage and mouse behaviour was recorded for 3 min. NoldusEthovision v3.1 behavioural analysis software was used to determine innate avoidance behaviour (time spent in the third of the cage containing the scented filter paper).

Full Methods and any associated references are available in the online version of the paper at www.nature.com/nature.

1. Sahin, E. & Depinho, R. A. Linking functional decline of telomeres, mitochondria and stem cells during ageing. *Nature* **464,** 520–528 (2010).
2. Whitman, M. C. & Greer, C. A. Adult neurogenesis and the olfactory system. *Prog. Neurobiol.* **89,** 162–175 (2009).
3. Sharpless, N. E. & DePinho, R. A. How stem cells age and why this makes us grow old. *Nature Rev. Mol. Cell Biol.* **8,** 703–713 (2007).
4. Ju, Z. & Lenhard Rudolph, K. Telomere dysfunction and stem cell ageing. *Biochimie* **90,** 24–32 (2008).
5. Hoeijmakers, J. H. DNA damage, aging, and cancer. *N. Engl. J. Med.* **361,** 1475–1485 (2009).
6. Ferrón, S. *et al.* Telomere shortening and chromosomal instability abrogates proliferation of adult but not embryonic neural stem cells. *Development* **131,** 4059–4070 (2004).
7. Cawthon, R. M. *et al.* Association between telomere length in blood and mortality in people aged 60 years or older. *Lancet* **361,** 393–395 (2003).
8. Wyllie, F. S. *et al.* Telomerase prevents the accelerated cell ageing of Werner syndrome fibroblasts. *Nature Genet.* **24,** 16–17 (2000).
9. Bodnar, A. G. *et al.* Extension of life-span by introduction of telomerase into normal human cells. *Science* **279,** 349–352 (1998).
10. Tomás-Loba, A. *et al.* Telomerase reverse transcriptase delays aging in cancer-resistant mice. *Cell* **135,** 609–622 (2008).
11. Samper, E., Flores, J. M. & Blasco, M. A. Restoration of telomerase activity rescues chromosomal instability and premature aging in $Terc^{-/-}$ mice with short telomeres. *EMBO Rep.* **2,** 800–807 (2001).
12. Metzger, D. *et al.* Conditional site-specific recombination in mammalian cells using a ligand-dependent chimeric Cre recombinase. *Proc. Natl Acad. Sci. USA* **92,** 6991–6995 (1995).
13. Blasco, M. A. *et al.* Telomere shortening and tumor formation by mouse cells lacking telomerase RNA. *Cell* **91,** 25–34 (1997).
14. Wong, K. K. *et al.* Telomere dysfunction and Atm deficiency compromises organ homeostasis and accelerates ageing. *Nature* **421,** 643–648 (2003).
15. Choudhury, A. R. *et al. Cdkn1a* deletion improves stem cell function and lifespan of mice with dysfunctional telomeres without accelerating cancer formation. *Nature Genet.* **39,** 99–105 (2006).
16. Best, B. P. Nuclear DNA damage as a direct cause of aging. *Rejuvenation Res.* **12,** 199–208 (2009).
17. Drapeau, E. & Nora Abrous, D. Stem cell review series: role of neurogenesis in age-related memory disorders. *Aging Cell* **7,** 569–589 (2008).
18. Ferrón, S. R. *et al.* Telomere shortening in neural stem cells disrupts neuronal differentiation and neuritogenesis. *J. Neurosci.* **29,** 14394–14407 (2009).
19. Enwere, E. *et al.* Aging results in reduced epidermal growth factor receptor signaling, diminished olfactory neurogenesis, and deficits in fine olfactory discrimination. *J. Neurosci.* **24,** 8354–8365 (2004).
20. Lafreniere, D. & Mann, N. Anosmia: loss of smell in the elderly. *Otolaryngol. Clin. North Am.* **42,** 123–131 (2009).
21. Ma, D. K. *et al.* Activity-dependent extrinsic regulation of adult olfactory bulb and hippocampal neurogenesis. *Ann. NY Acad. Sci.* **1170,** 664–673 (2009).
22. Kobayakawa, K. *et al.* Innate versus learned odour processing in the mouse olfactory bulb. *Nature* **450,** 503–508 (2007).
23. Caporaso, G. L. *et al.* Telomerase activity in the subventricular zone of adult mice. *Mol. Cell. Neurosci.* **23,** 693–702 (2003).
24. Artandi, S. E. & DePinho, R. A. Telomeres and telomerase in cancer. *Carcinogenesis* **31,** 9–18 (2010).
25. Zhang, P., Dilley, C. & Mattson, M. P. DNA damage responses in neural cells: focus on the telomere. *Neuroscience* **145,** 1439–1448 (2007).
26. Lee, J. *et al.* Telomerase deficiency affects normal brain functions in mice. *Neurochem. Res.* **35,** 211–218 (2010).
27. Breton-Provencher, V. *et al.* Interneurons produced in adulthood are required for the normal functioning of the olfactory bulb network and for the execution of selected olfactory behaviors. *J. Neurosci.* **29,** 15245–15257 (2009).

METHODS

Generation of TERT-ER mice. A knock-in targeting vector containing the ERT2-LBD domain upstream and in frame with the *mTert* genomic sequence (exon 1 through intron 2) and a *Lox-pgk-Neo-Lox* fragment was introduced into ES cells. Neomycin-resistant clones yielded five independent lines, two of which were injected into C57BL/6 blastocysts and implanted into surrogate mothers, yielding 10 high-percentage chimaeras. Germline transmission was confirmed by crossing the chimaeras to C57BL/6 females. Heterozygous TERT-ERneo animals were crossed to EIIa-Cre animals to delete the NeoR cassette and further intercrossed to homozygosity. The EIIa-Cre allele was then bred out of the line and heterozygous animals were backcrossed to C57BL/6 at least three times. From this point, standard breeding protocol of successive generations of telomerase-deficient mice was followed[13,28]. All studies were performed on adult (30–35-week-old) males, heterozygous (G0$^{TERT-ER}$) or homozygous (G4$^{TERT-ER}$) for this allele, unless otherwise noted. 4-OHT time-release pellets (2.5 mg; Innovative Research of America) were inserted subcutaneously to reach steady state blood levels of 1 ng ml^{-1} 4-OHT. Mice were maintained in specific pathogen-free (SPF) conditions at Dana-Farber Cancer Institute. All manipulations were performed with IACUC approval.

Histology and electron microscopy. Brains from animals perfused with 10% formalin were further fixed for 24 h and coronally sectioned using a brain matrix (Electron Microscopy Sciences). Equivalent sections were used for chromogenic immunohistochemistry, which was performed according to standard procedures. Antibodies used include anti-Ki67 (Dako), anti-53BP1 (Bethyl Labs), anti-Sox-2 and anti-Dcx (Santa Cruz Biotechnology) and anti-Olig-2 (Chemicon). For immunofluorescence studies, cells were fixed in 4% paraformaldehyde (PFA) in phosphate-buffered saline for 10 min, permeabilized (50 mM NaCl, 3 mM MgCl$_2$, 200 mM sucrose, 10 mM HEPES pH 7.9, 0.5% TX-100) for 5 min, and then stained with primary antibodies against 53BP1 (Bethyl Labs), TUJ1 (Chemicon), GFAP (Dako) and secondary antibodies conjugated to Alexa Fluor-488 or Alexa Fluor-568 (Molecular Probes). Cells were mounted in DAPI-containing antifade solution (Vector). Foci were scored by eye from a minimum of 300 randomly chosen nuclei by using a ×40 objective, and scoring was performed in a blinded manner with respect to genotype. Immunofluorescence images were captured in greyscale for each fluorophore and were merged by compilation in respective red-green-blue (RGB) channels using Adobe Photoshop CS 8.0. For apoptosis assays, sections from paraffin-embedded testes were deparaffinized and processed for apoptotic staining (terminal deoxynucleotidyl transferase-mediated dUTP-biotin nick end labelling, TUNEL) according to the manufacturer's instructions (Chemicon). For electron microscopy studies, animals were perfused for 30 min in Karnovsky's solution B, brains were further fixed for 24 h and delivered to the Harvard Medical School Electron Microscopy Facility for embedding, sectioning and staining. Electron micrographs were generated using a JEOL 1200EX microscope and analysed with ImageJ software[29]. Inner and outer diameters were analysed as per ref. 30.

Assessment of telomerase activity. Telomeric repeats amplification protocol (TRAP) was combined with real-time detection of amplification products to determine telomerase activity with a Quantitative Telomerase Detection kit (US Biomax) following the manufacturer's recommendations. Total protein extract (0.5 µg) was used in each reaction. End products were resolved by PAGE in a 12.5% non-denaturing gel, stained with Sybr Green Nucleic Acid gel stain (Invitrogen) and visualized with a Bio-Rad Molecular Imager ChemiDoc System.

Cell culture and cytogenetic analysis. Ear skin fibroblasts were isolated as described previously[31]. Proliferation assays were carried in triplicate on 6-well plates. Cells were grown in RPMI-10% fetal calf serum-50 µM β-mercaptoethanol with the addition of 100 nM 4-OHT or vehicle (ethanol). Cells were counted and replated at a density of 1,000 cells per well every 4 days. Splenocytes were isolated by generating single-cell suspensions from whole spleen, stimulated for 48 h with 2.5 µg ml^{-1} concavalin A and 20 µg ml^{-1} LPS (Sigma) and treated with KaryoMAX Colcemid solution (Invitrogen) for 2 h before collection. Telomere fluorescence *in situ* hybridization (FISH) was performed on metaphase nuclei as described previously[28]. At least 15 metaphases from harvested cell cultures were analysed for telomere integrity by telomere-specific peptide nucleic acid (PNA)-FISH. Telomere signal was normalized using a Pacific Blue centromeric PNA probe. For telomere-tissue-FISH, frozen tissue sections (8-µm thick) were fixed in 2% PFA for 15 min and permeabilized in 0.5% Triton X-100 for 10 min. Two PNA probes, telomere-specific FITC-00-T2AG3 and Pacific Blue-centromere-specific, were hybridized after 4 min denaturing at 83 °C under the following conditions: 70% formamide, 0.06× SSC, 0.2% BSA, 0.5 ng µl^{-1} tRNA, 0.5 ng µl^{-1} PNA probe; overnight at 25 °C. To achieve uniform hybridization we used MAUI Mixer (BioMicro) with 40 µl chamber. Nuclei were stained with TOTO3 (Invitrogen) far red stain. Telomere signal was normalized using the centromeric PNA probe. For neurosphere assays, subventricular region of brain from 3- to 6-week-old mice was dissected, dispersed into a single-cell suspension and plated in neurobasal media (StemCellTechnologies) supplemented with EGF and bFGF (20 ng ml^{-1} each) for 4 days, in the presence of 100 nM 4-OHT or vehicle (ethanol). Primary neurospheres were dissociated and seeded at 2 cells per µl density in multi-well plates. After 7–10 days, cultures were monitored for the formation of neurospheres. Alternatively, single cells were sorted into individual wells on 384-well plates at a density of 10 cells per well on Dako MoFlo high-speed cell sorter and grown for 3 weeks. Neurospheres were transferred to culture wells coated with poly-L-ornithine (15 µg ml^{-1}) and fibronectin (1 µg ml^{-1}) and differentiated in 1% FBS in neurobasal media to measure their multipotentiality. Quantification of neurosphere numbers and diameters were performed by bright-field microscopy coupled with an in-house semi-automated segmentation algorithm generated with MATLAB software (The Mathworks). For multipotentiality assays, cells were fixed, stained with GFAP and TUJ1 antibodies and quantified as described previously[32].

Laser scanning analysis for the quantification of IHC and FISH. Laser scanning cytometry quantification was performed with an iCys Research Imaging Cytometer (Compucyte) as described earlier[32,33,34] with a few modifications. Counts of Ki67$^+$, Dcx$^+$ or Sox2$^+$ cells (DAB positive) were carried out within the subventricular zones that were predefined by a certified pathologist with the haematoxylin and eosin-stained brain architecture. The target number for each sample was approximately 500 cells counted. Olig2$^+$ cell within the corpus callosum were counted in a similar manner.

RT–PCR, Southern blotting and western blotting. DNase-treated total RNA extracted from fresh liver samples with the RNeasy kit (Qiagen) was used to prepare oligo-dT complementary DNA with Superscript III (Invitrogen). RT–PCR primers are described in Supplementary Table 3. Southern and western blots were performed following standard techniques. For western blots, 40 µg protein were loaded per lane. Antibodies used include phospho-p53 (Ser15, Cell Signaling Technologies), p21 (Santa Cruz Biotechnology), Actin (Biolegend) and horseradish peroxidase-conjugated secondary antibodies (Pierce/ThermoScientifics).

Innate olfactory avoidance test. Animals were kept in a 12-h light/dark cycle and tested in the second half of the light cycle. Male mice (30–35-week-old, $n = 4$ per experimental condition) were fasted for 20 h before testing. To avoid confounding of data owing to learning, mice were used only once. To habituate to the experimental environment, mice were placed individually in a cage that was identical to the test cage (259 × 476 × 209 mm) for 20 min before the onset of testing. Following acclimation, mice were placed in an identical test chamber where their responses were recorded on a video camera (30 frames per second, 640 × 480 pixels) mounted above the test chamber. Confounding environmental/spatial cue effects were ruled out by monitoring total time spent in different zones of the chamber in the absence of odorants. For innate avoidance tests, circular filter paper (2.5 cm diameter) was scented with 40 µl of either water or progressively higher concentrations of 2-MB (1.74×10^{-6} M to 1.74×10^{-4} M) and mouse behaviour was recorded for 3 min. Videos were transferred to computer for subsequent analysis using NoldusEthovision v3.1 behavioural analysis software[35]. First the cage was divided into thirds and then time spent in each third for the duration of the recording was determined using the software. Total distance travelled, frequency of entry into the third containing the filter paper treated with the odorants (zone 3) as well as time spent investigating in this zone (to determine innate avoidance behaviour) was collated for each treatment and genotype.

Statistical analysis. All the data were analysed by one way ANOVA with Bonferroni's post test (significantly different at $P < 0.05$). Survival curves were analysed with Mantel–Cox test.

28. Maser, R. S. *et al.* DNA-dependent protein kinase catalytic subunit is not required for dysfunctional telomere fusion and checkpoint response in the telomerase-deficient mouse. *Mol. Cell. Biol.* **27,** 2253–2265 (2007).
29. Abramoff, M. D., Magelhaes, P. J. & Ram, S. J. Image Processing with ImageJ. *Biophotonics Int.* **11,** 36–42 (2001).
30. Potzner, M. R. *et al.* Prolonged Sox4 expression in oligodendrocytes interferes with normal myelination in the central nervous system. *Mol. Cell. Biol.* **27,** 5316–5326 (2007).
31. Shao, C. *et al.* Mitotic recombination produces the majority of recessive fibroblast variants in heterozygous mice. *Proc. Natl Acad. Sci. USA* **96,** 9230–9235 (1999).
32. Paik, J. H. *et al.* FoxOs cooperatively regulate diverse pathways governing neural stem cell homeostasis. *Cell Stem Cell* **5,** 540–553 (2009).
33. Mahoney, J. E. *et al.* Quantification of telomere length by FISH and laser scanning cytometry. *Proc. SPIE* **6859,** 1–9 (2008).
34. Gorczyca, W. *et al.* Analysis of human tumors by laser scanning cytometry. *Methods Cell Biol.* **64,** 421–443 (2001).
35. Spink, A. J. *et al.* The EthoVision video tracking system–a tool for behavioral phenotyping of transgenic mice. *Physiol. Behav.* **73,** 731–744 (2001).